Research Article

Yu Zhao*, Ashok Kumar, Giti A. Khodaparast, Amnah Eltahir, Hsin Wang, and Shashank Priya

Sintering Temperature-Dependent Chemical Defects and the Effect on the Electrical Resistivity of Thermoelectric ZnO

Abstract: Thermoelectric properties of zinc oxide (ZnO) are largely influenced by its electrical property. In this paper, we investigated the correlation between the electrical resistivity and synthesis temperature for aluminum (Al)-modified ZnO. At constant Al doping, the electrical resistivity of ZnO exhibited sharp decrease with increase in sintering temperature due to the increased carrier density resulting from Al^{3+} substitution on Zn^{2+} sites. Photoluminescence analysis showed that segregation of Al in secondary phase, $ZnAl_2O_4$, promotes Zn^{2+} vacancy formation and consequently compensates the free electrons that dominate the electrical behavior at relatively low sintering temperature. The mechanism controlling the large change in electrical resistivity of dense ZnO, ranging from insulator (~10^7 Ω cm) to semiconducting regime (~ 0.1 Ω cm) has been discussed.

Keywords: Al-doped ZnO, electrical resistivity, carrier density, sintering temperature, defect chemistry, thermoelectric

***Corresponding author: Yu Zhao,** Bio-Inspired Materials and Devices Laboratory (BMDL), Center for Energy Harvesting Materials and Systems (CEHMS), Virginia Tech, 310 Durham Hall, MC 0261, Blacksburg, VA 24061, USA, E-mail: zhaoyu@vt.edu
Ashok Kumar, Bio-Inspired Materials and Devices Laboratory (BMDL), Center for Energy Harvesting Materials and Systems (CEHMS), Virginia Tech, 310 Durham Hall, MC 0261, Blacksburg, VA 24061, USA, E-mail: ashokku@vt.edu
Giti A. Khodaparast: E-mail: khoda@vt.edu, **Amnah Eltahir:** E-mail: amnah@vt.edu, Department of Physics, Virginia Tech, Blacksburg, VA 24061, USA
Hsin Wang, Division of Materials Science and Technology, Oak Ridge National Laboratory, Oak Ridge, TN 37831, USA, E-mail: wangh2@ornl.gov
Shashank Priya, Bio-Inspired Materials and Devices Laboratory (BMDL), Center for Energy Harvesting Materials and Systems (CEHMS), Virginia Tech, 310 Durham Hall, MC 0261, Blacksburg, VA 24061, USA, E-mail: spriya@vt.edu

Introduction

For high thermal to electric energy conversion efficiency, thermoelectric (TE) materials with large figure of merit (ZT) and good stability at elevated temperature are required, where $ZT = \alpha^2\sigma T/\kappa$, α is the Seebeck coefficient, σ is the electrical conductivity, κ is the thermal conductivity, and T is the absolute temperature. ZnO is a naturally occurring n-type wide-band gap semiconductor (Ohtaki et al. 1996) exhibiting good Seebeck coefficient and substantial durability at elevated temperature in air (Koumoto et al. 2006). ZnO is considered as a promising thermoelectric material; however, similar to other oxide TE materials, it exhibits low electrical conductivity due to relatively low carrier concentration and mobility. Previous studies from Ohtaki et al. (1996) and Tsubota et al. (1997) revealed that the electrical conductivity of Al_2O_3-modified ZnO can be increased by more than three orders of magnitude in comparison to undoped ZnO. Studies on the ZnO bulk and thin film have shown that this enhancement occurs due to the Al^{3+} substitution on Zn^{2+} site, which creates an extra electron if the charge is not compensated by adsorption of excess stoichiometric oxygen or formation of Zn^{2+} vacancies (Cai et al. 2003; Singh et al. 2004; Zhan et al. 2011). The solubility of Al_2O_3 in ZnO is limited (Shirouzu et al. 2007) of the order of ~0.3 at% at 1,400°C. Experiments from Tsubota et al. (1997) showed that higher concentration of Al_2O_3 in ZnO has negligible effect on the magnitude of electrical conductivity; however, there was no detailed discussion on this phenomenon. To improve the carrier concentration, Kim et al. (2005) investigated the effect of co-doping of Al and Ni, yet there was only slight increase in the electrical conductivity. Later Ohtaki, Araki, and Yamamoto (2009) reported higher solubility limit of Al in ZnO through Ga co-doping, nevertheless, there was only slight improvement in the electrical conductivity also. Despite the challenges, aluminum still remains the most common and important dopant for ZnO (Özgür et al.

2005). Recently, Berardan, Byl, and Dragoe (2010) have shown that Al-doped ZnO samples sintered in nitrogen atmosphere have electrical conductivity higher than those sintered in air due to the native defects introduced by low-oxygen partial pressure. It is imperative from these prior studies that both effective doping concentration and sintering atmosphere modifies the defect chemistry in ZnO and thereby affects the electrical property. However, the mechanism for conductivity changes occurring by doping Al_2O_3 in bulk ZnO beyond solubility limit is still not clear.

Recently, significant progress has been achieved in design of thermoelectric materials with high *ZT* by incorporating nanostructures (Snyder and Toberer 2008). The nanostructures in ZnO have been shown to reduce its thermal conductivity (Zhao et al. 2012). Generally, to achieve nanostructure in bulk ZnO, lower synthesis temperature is required. However, a comprehensive study investigating the influence of sintering temperature on electrical conductivity is lacking. Han, Mantas, and Senos (2001) found that the electrical conductivities of ZnO-Al sintered at 1,100°C and 1,400°C exhibited difference of 50 times. In Al-modified ZnO, Al mainly occupies the Zn site or forms a secondary phase (Tsubota et al. 1997). With varying temperature, the phase diagram governs the phase evolution between ZnO and Al_2O_3 and thus selection of specific sintering temperature is also critical toward defining the role of Al in ZnO. In order to achieve comprehensive understanding of the electrical behavior of Al-modified ZnO, a systematic study of the electrical resistivity and defect chemistry as a function of sintering temperature was performed. The measured values of electrical resistivity revealed a large variation as a function of sintering temperature. The results of this study have significant implications toward design of ZnO ceramics for thermoelectric applications.

Methods

ZnO modified with 2 at% Al (ZnO-Al) were synthesized using nano-size precursor powders of ZnO (~30 nm, purity > 99.7%, Advanced Materials LLC) and Al_2O_3 (40–50 nm, purity > 99.5%, Alfa Aesar) through solid-state reaction. The mixed powders were pelletized and consolidated using cold isostatic pressing (CIP) at 200 MPa and then sintered at 950, 1,100, 1,200, 1,300, 1,400°C for 5 h in air. The density of the samples was measured to be 5.37, 5.48, 5.48, 5.47, and 5.44 g/cm^3 respectively using Archimedes' method. The phase(s) and microstructure of the samples were examined using X-ray diffraction (XRD, PANalytical X'Pert, CuKa; Philips, Almelo, the Netherlands) and scanning electron microscopy (SEM, LEO (Zeiss) 1550 field-emission). Electrical resistivity was measured by van der Pauw method (Keithley 4200-SCS) for relatively low resistivity samples and by voltage–current method using Precision Premier II tester (Radiant Technologies) for samples with high resistivity. The resistivity at varying temperature of the ZnO-Al sintered at 1,400°C was also determined by ZEM-3 Seebeck coefficient/Electric resistance measuring system. Impedance measurements were performed using Versa STAT 3 analyzer as a function of frequency (0.1 Hz to 1 MHz). The Hall Effect measurements were conducted in the Van der Pauw geometry to determine the carrier density. An UV-Vis-NIR spectrophotometer (Hitachi U 4100) was used for absorbance measurement. The PL spectra were collected using luminescence spectrometer (Perkin-Elmer, LS50B, USA) equipped with a 200 W Xe lamp and red-sensitive photomultiplier tube (Hamamatsu, R928, Japan).

Results and discussion

XRD patterns of ZnO-Al samples as a function of sintering temperature are shown in Figure 1. These patterns show the formation of a hexagonal wurtzite-type zinc oxide phase (JCPDS # 36–1451) and a small fraction of the gahnite phase, $ZnAl_2O_4$ (JCPDS # 5-0669) (Figure 1b). Figure 1c shows the change of unit cell volume of ZnO-Al samples sintered in the temperature range of 950–1,400°C. When the sintering temperature increased from 950 to 1,200°C, an increase in unit cell volume was noticed. The smaller unit cell volume below 1,200°C sintering temperature was probably caused by the dissolution of ZnO in Al_2O_3 and formation of $ZnAl_2O_4$ phase. With increase in sintering temperature from 1,200 to 1,400°C, there was a slight decrease in unit cell volume, likely because the solubility of Al in ZnO rises with temperature according to the phase diagram of ZnO-Al_2O_3. With increasing temperature, more Al^{3+} ions occupy the Zn^{2+} sites and consequently lead to the decrease in the volume of unit cell, as ionic radius of Al^{3+} (0.39 Å) in fourfold coordination is smaller than Zn^{2+} (0.60 Å).

The SEM images of the ZnO-Al ceramic are displayed in Figure 2a. All samples were found to exhibit dense microstructure except the ones sintered at 950°C, which agrees with the measured densities. The average grain size increases exponentially with sintering temperature (Senda and Bradt 1990) as shown in Figure 2b. A small

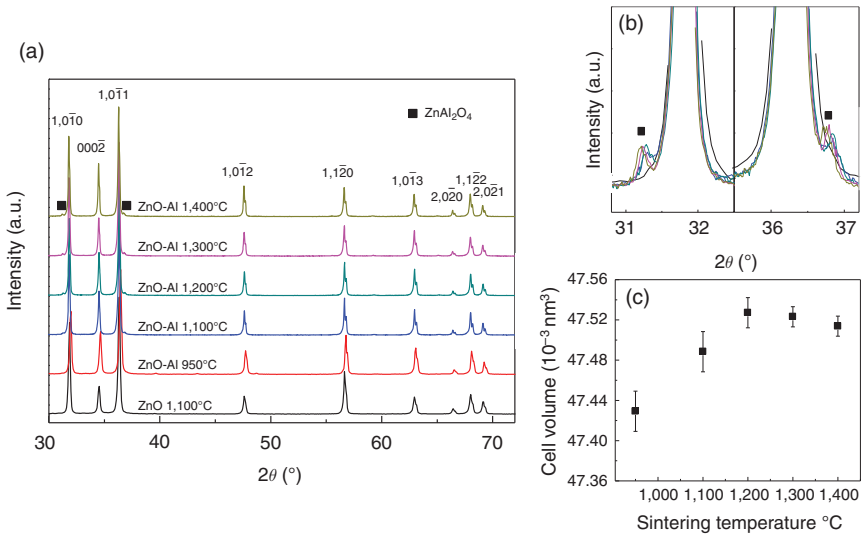

Figure 1 (a) XRD pattern of ZnO-Al sintered at different temperatures and compared with the pure ZnO sintered at 1,100°C; (b) higher magnification of the XRD pattern (c) the unit cell volume changes of ZnO-2%Al sintered at different temperatures

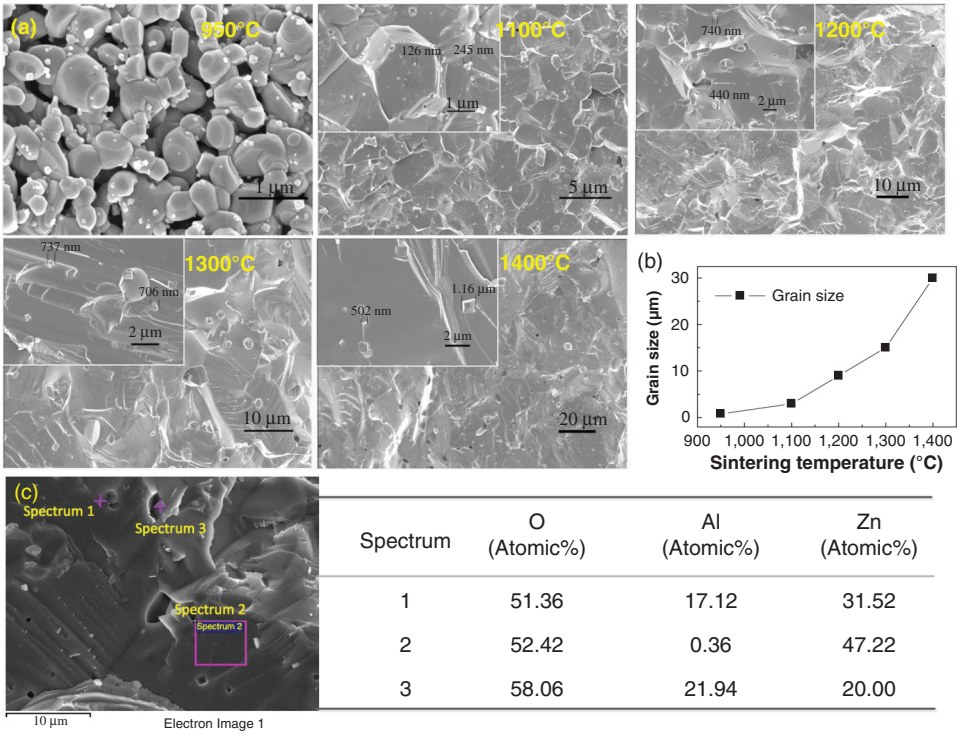

Spectrum	O (Atomic%)	Al (Atomic%)	Zn (Atomic%)
1	51.36	17.12	31.52
2	52.42	0.36	47.22
3	58.06	21.94	20.00

Figure 2 (a) and (b) SEM and grain size of ZnO-Al sintered at different temperatures; (c) EDS element scanning of ZnO-Al sintered at 1,300°C. Atomic element compositions are included in the figure

amount of second-phase precipitates can be observed in all the ZnO-Al samples (insert figures of Figure 2a). At higher sintering temperature, precipitates with larger size were observed in the microstructure. The element scanning on a typical ZnO-Al sample sintered at 1,300°C confirmed that the distribution of aluminum is richer in the precipitate phase (spectrum 1 and 3) as compared to the matrix ZnO (spectrum 2) as shown in Figure 2c.

Electrical resistivity (ρ) of ZnO-Al samples exhibited significant variations as a function of sintering temperature as shown in Figure 3a. The higher value of ρ at lower sintering temperature (950°C) might be attributed to the

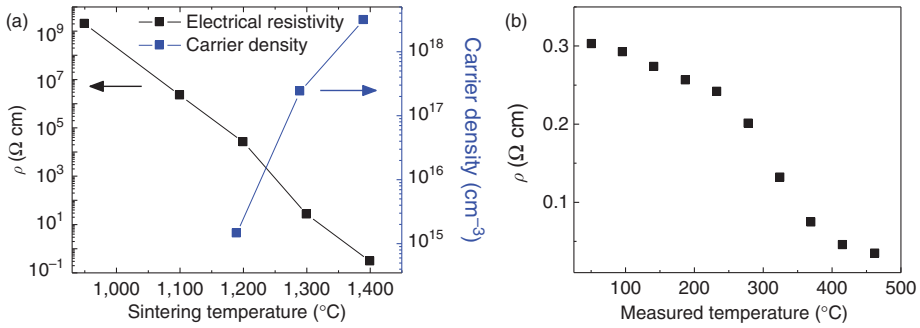

Figure 3 (a) Electrical resistivity and carrier density of ZnO-Al sintered at different temperatures; (b) Electrical resistivity of ZnO-Al sintered at 1,400°C as a function of measurement temperature

porous microstructure (Figure 2a). The densities for the samples synthesized in the temperature range of 1,100–1,400°C are similar and therefore not a deterministic parameter. With increase in sintering temperature, the values of electrical resistivity decreased sharply. According to the Hall effect measurements (Figure 3a), the main reason for electrical conductivity enhancement with temperature is related to the increase in carrier density. The carrier density values of ZnO-Al synthesized at relatively low temperature (<1,200°C) are not provided since the carrier concentration was low. The variation of ρ as a function of measurement temperature for the typical ZnO-Al synthesized at 1,400°C shows the decreasing trend with increase in temperature (Figure 3b). Assuming the carrier concentration is constant with measurement temperature, the carrier mobility in the grain is determined by the impurity (doping ions). The impurity scattering decreases at higher temperature while the scattering from lattice increases with temperature. Therefore, the ZnO-Al samples had higher concentration of impurities, such as dopant, vacancies, or interstitial atoms.

To understand the variation of resistance in the interior of the grain and at the grain boundary, impedance measurements were conducted as shown in Figure 4. The impedance spectrum of ZnO-Al sample sintered at 1,100°C exhibited two overlapping semicircles. The high-frequency (low magnitude of real component Z') and the low frequency (high magnitude of real component Z') correspond to the grain interior (with $ZnAl_2O_4$ precipitates) and grain boundary resistance respectively. At higher sintering temperature, the impedance spectra displayed a single oblate arc, as the time constants for grain interior and grain boundary were identical. The equivalent circuit fitting results [displayed in supplemental material] showed good matches with measured plots and parameters are listed in Table 1. After sintering at higher temperature, samples' resistance and capacitive reactance ($(2\pi fC)^{-1}$) from both grain interior and grain boundary decreased sharply, and the corresponding frequency (f_{max}) increased. These indicate the enhancement in electron mobility through grain interior and grain boundary. Both R_g and R_{gb} significant decreases

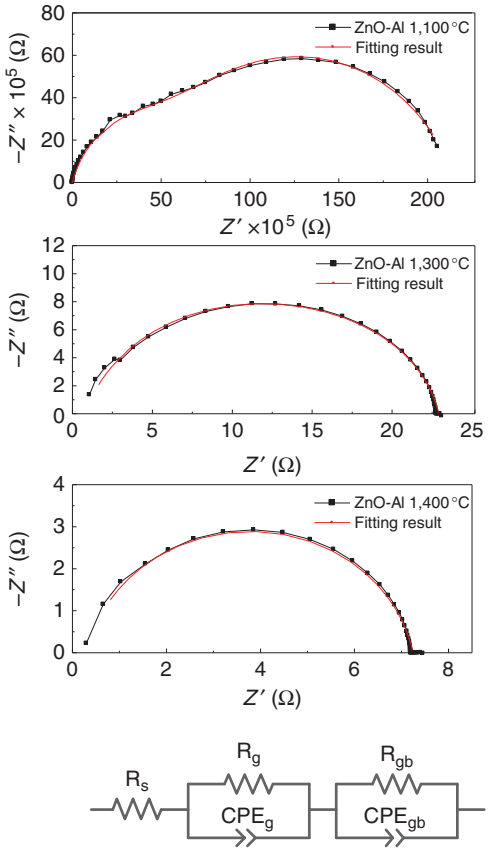

Figure 4 The impedance spectra and SEM micrographs of ZnO-Al sintered at different temperatures. The results are fitted with an equivalent circuit model shown by red line

Table 1 Parameters obtained by equivalent circuit model fitting of the impedance data

Sintering temperature (°C)	1,100	1,300	1,400
R_g (Ω)	5.0×10^6	8.9	1.0
CPE-T_g (nF)	2.8	2.2×10^2	3.6×10^3
CPE-P_g	0.83	0.97	0.94
$f_g$max (Hz)	11.4	8.13×10^4	4.42×10^4
R_{gb} (Ω)	1.7×10^7	13.1	5.9
CPE-T_{gb} (nF)	14.1	1.9×10^3	1.4×10^3
CPE-P_{gb}	0.76	0.89	0.87
f_{gb}max (Hz)	0.664	6.4×10^3	1.93×10^4
R_s (Ω)	1.9×10^{-9}	1.0	0.3

contribute to the overall lower magnitude of electrical resistivity at relatively higher sintering temperature. Considering that the thickness of grain boundary is smaller than the grain interior of ZnO-Al, the grain boundary should have larger resistivity than the grain interior, which plays an important role toward electrical resistivity.

Due to large distinction of carrier concentration (n), the variation of electrical resistivity of samples can be understood through changes in defect chemistry (defects created by doping and intrinsic defects). To better understand the doping effects of Al, absorbance spectra of ZnO-Al samples in the wavelength range of 200–1,000 nm were collected as shown in Figure 5. These spectra revealed slight red shift of absorption edge with increase in sintering temperature. Based on the double derivative of absorbance spectra (insert of Figure 5a), the effective band gap of doped ZnO was calculated and the values were found to slightly increase from 3.09 eV for the ZnO-Al sample sintered at 1,100°C to 3.16 eV for the one sintered at 1,400°C. The widening of the effective band gap in the samples sintered at higher temperature was consistently observed. As shown in the schematic band structure in Figure 5b and c, the associated electrons released from ionized Al atoms occupying the bottom of the conduction band widen the optical band gap. This is commonly known as Burstein–Moss Effect (Burstein 1954). The blocking of the lowest states in the conduction band enhances the effective band gap as (Sernelius et al. 1988):

$$\Delta E_g^{\text{Burstein-Moss}} = \frac{h^2 k_F^2}{2}\left[\frac{1}{m_e} + \frac{1}{m_h}\right] \quad [1]$$

where k_F is the Fermi wave vector, m_e and m_h are the effective mass for electrons in conduction band and holes for valence band. The same phenomenon was reported in Al-doped ZnO thin film by Sernelius et al. (1988). Higher electron concentration in conduction band probably results from the defects created through Al doping, which is consistent with the unit cell volume calculated from XRD. More Al atoms dissolve in the ZnO at higher synthesis temperature resulting in slight unit cell shrinkage.

The concentration of the intrinsic defects varies with the sintering temperature as well. Studies on ZnO have shown that the intrinsic defects play an important role on the electrical property (Özgür et al. 2005). The photoluminescence (PL) spectra at the excitation wavelength of 325 nm for the ZnO-Al samples are shown in Figure 6. The PL intensity reduced with increasing sintering temperature owning to the carrier density enhancement. Lupan et al. (2009) have reported that the increase of carrier density results in the PL intensity augmentation. This again affirms the above discussion that Al doping concentration in ZnO lattice increases resulting in the enhancement of the carrier density. The green

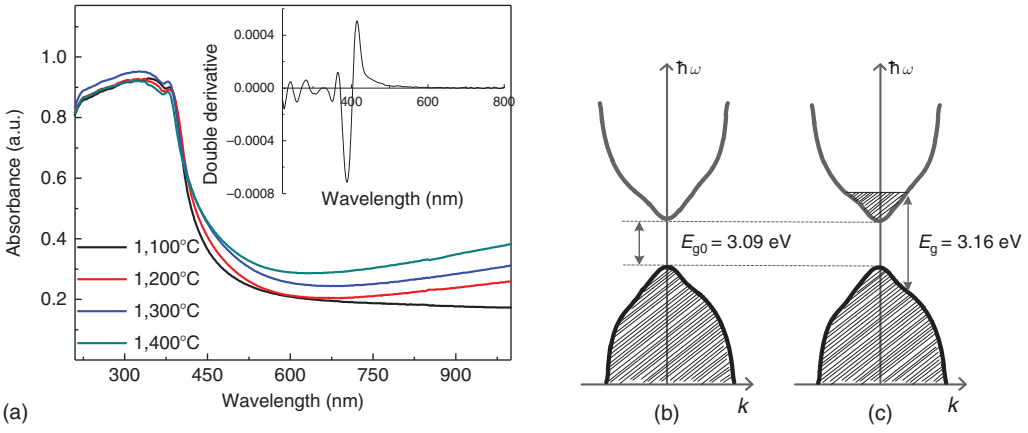

Figure 5 (a) UV-VIS-NIR spectra of ZnO-Al sintered at different temperatures and inset is double derivative of the absorbance for band gap; (b) Schematic band structure of ZnO with parabolic conduction and valence bands; (c) Schematic band structure of Al-doped ZnO

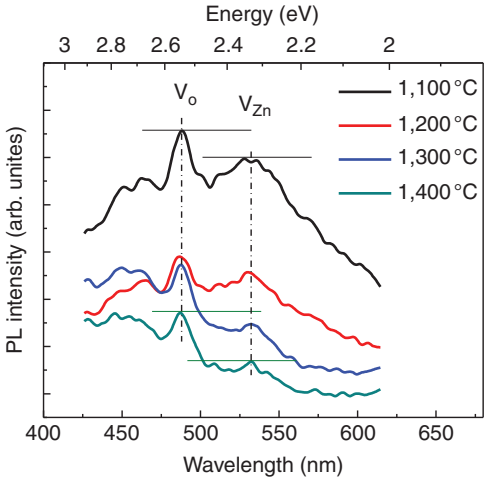

Figure 6 The PL spectra of ZnO-Al sintered at different temperatures. The emission energy representing the zinc vacancies and oxygen vacancies is shown in the figure

luminescence or deep band emissions observed at 2.5 and 2.35 eV was attributed to the oxygen vacancy (V_O) and zinc vacancy (V_{Zn}) (marked in Figure 6). V_{Zn} has been reported to be the source of green emission at 2.35 eV and V_O at 2.42–2.53 eV in several earlier studies Børseth et al. (2006), Willander et al. (2010) and Vanheusden et al. (1996). The broad spectral distribution of oxygen vacancies indicates that hybridization may be occurring that results in redistribution of the energy widening the range of these defects. The presence of oxygen vacancies was further confirmed by thermally stimulated depolarization current (TSDC) measurements [data included in the supplemental material]. The PL intensity ratio of 480 and 535 nm peaks increased (the emission intensity difference from V_O and V_{Zn} increases) with higher sintering temperature indicating the relative decrease in population of Zn vacancies. The population of Zn vacancies increased with decrease in sintering temperature, which is in agreement with the measured changes in the cell volume. As the electron acceptor, V_{Zn}^{2-} and V_{Zn}^{-} compensate free electrons and in turn contribute toward the reduction of the overall electrical conductivity (Willander et al. 2010). In general, ZnO is a native n-type semiconductor; thereby, the V_{Zn} appearance is an important factor for high resistivity of ZnO-Al ceramics sintered at relatively low temperature. Whether oxygen vacancies contribute to the carrier density is still under investigation due to the high energy of formation (Özgür et al. 2005).

Above-mentioned results provide the explanation for large changes in resistivity with sintering temperatures in Al_2O_3-modified ZnO. In the solid-state reaction of ZnO and Al_2O_3, there are two most likely reactions, namely, Al^{3+} substitution on Zn^{2+} and Al^{3+} forming the gahnite phase (Cai et al. 2003; Singh et al. 2004; Zhan et al. 2011; Berardan, Byl, and Dragoe 2010). These reactions can be expressed as:

$$Al_2O_3 \overset{Zno}{\rightarrow} 2Al_{Zn}^{\bullet} + 2e' + 2O_o^{\times} + \frac{1}{2}O_2 \quad [2]$$

$$ZnO + Al_2O_3 \rightarrow ZnAl_2O_4 \quad [3]$$

$$Al_2O_3 + (Zn_{Zn}^{x} + 2e' + \frac{1}{2}O_2)_{ZnO} \rightarrow ZnAl_2O_4 + (V''_{Zn})_{ZnO} \quad [4]$$

The dissolved Al^{3+} acts as a donor and subsequently enhances the electrical conductivity according to eq. [2]. Native defects are formed due to the formation of secondary phase, the gahnite phase ($ZnAl_2O_4$) that is precipitated during the sintering in ZnO-Al samples as shown by eq. [3] due to the limited solubility of Al_2O_3 in ZnO. This preferably promotes the generation of Zn^{2+} vacancies (eq. [4]) (required oxygen for $ZnAl_2O_4$ phase formation may be obtained from air) which, in turn, compensates the free carriers and subsequently reduces the electrical conductivity. All the reactions shown in eqs [2]–[4] occur simultaneously and their relative contributions vary with the synthesis temperature. At low sintering temperature, such as 1,100°C, the reaction [3] or [4] is prevalent; therefore, most of the alumina is consumed toward the formation of $ZnAl_2O_4$ phase. For this reason, the concentration of Al^{3+} ions occupying the ZnO lattice is very small, and any reverse dissolution of Zn^{2+} into Al_2O_3 creates Zn vacancies that further compensate the free electrons. This reaction is well supported by the XRD measurements showing the unit cell dimension changes. Thus, the ZnO-Al samples sintered at relatively low temperature exhibits much higher resistivity than that sintered at higher temperature. With increase in sintering temperature, higher fraction of Al^{3+} ions occupy Zn site releasing free electrons at shallow energy level resulting in higher carrier concentration. Related to the impedance spectrum, the decrease of ρ_g with increase in sintering temperature is mainly due to the increase of Al incorporation in ZnO matrix. The decrease of ρ_{gb} occurs due to enhanced Al doping at higher sintering temperature, reduced grain boundary area, and better lattice arrangement during at higher sintering temperature.

In summary, this paper shows the effect of sintering temperature on the electrical resistivity of zinc oxide thermoelectric. Dense ZnO-Al samples exhibited a large difference in electrical resistivity ranging from insulator

(~10^7 Ω cm) to semiconductor (~0.1 Ω cm). Both the resistivity of grain interior and the grain boundary were found to reduce significantly with sintering temperature. At lower temperature, Al mainly exists in the secondary phase $ZnAl_2O_4$, which promotes the formation of Zn^{2+} vacancy and consequently decreases the carrier density. With increase in sintering temperature, higher concentration of Al incorporates in the ZnO, releasing electron carriers. In order to synthesize ZnO with low thermal conductivity by nanostructures and high electrical conductivity, synthesis techniques that can achieve high doping concentration at relatively low temperature are required. Chemical synthesis technique would be one such possibility to achieve uniform mixture of Al-ZnO and thus enhance the concentration of Al in ZnO (Jood et al. 2011).

Acknowledgment: Authors gratefully acknowledge the financial support provided by NSF/DOE Thermoelectric Partnership program and would like to thank Dr. Hao-Hsiang Liao, Zhenbo Xia and Dr. BoYun Jang for the help with the Van der Pauw method, Impedance and PL measurement, and Dr. Yongke Yan for his helpful suggestions. G. A. Khodaparast would like to thank Doug Wilson for his helps with the lab view programming and acknowledge the support of NSF-REU supplement as part of the NSF-Career Award DMR-0846834.

References

Berardan, D., C. Byl, and N. Dragoe. 2010. "Influence of the Preparation Conditions on the Thermoelectric Properties of Al-Doped ZnO." *Journal of the American Ceramic Society* 93:2352.

Børseth, T. M., B. G. Svensson, A. Yu, K., P. Klason, Q. Zhao, and M. Willander. 2006. "Identification of Oxygen and Zinc Vacancy Optical Signals in ZnO." *Applied Physics Letters* 89:262112.

Burstein, E. 1954. "Anomalous Optical Absorption Limit in InSb." *Physical Review* 93:632.

Cai, K. F., E. Müller, C. Drašar, and A. Mrotzek. 2003. "Preparation and Thermoelectric Properties of Al-Doped ZnO Ceramics." *Materials Science and Engineering B* 104:45.

Han, J. P., P. Q. Mantas, and A. M. R. Senos. 2001. "Effect of Al and Mn Doping on the Electrical Conductivity of ZnO." *Journal of the European Ceramic Society* 21:1883.

Jood, P., R. J. Mehta, Y. Zhang, G. Peleckis, X. Wang, R. W. Siegel, T. Borca-Tasciuc, S. X. Dou, and G. Ramanath. 2011. "Al-Doped Zinc Oxide Nanocomposites with Enhanced Thermoelectric Properties." *Nano Letters* 11:4337.

Kim, K. H., S. H. Shim, K. B. Shim, K. Niihara, and J. Hojo. 2005. "Microstructural and Thermoelectric Characteristics of Zinc Oxide-Based Thermoelectric Materials Fabricated Using a Spark Plasma Sintering Process." *Journal of the American Ceramic Society* 88:628.

Koumoto, K., I. Terasaki, T. Kajitani, M. Ohtaki, and R. Funahashi. 2006. "Oxide Thermoelectrics." In D. M. Rowe (Ed.), *Thermoelectrical Handbook Macro to Nano*, 1st ed. New York: D.M. Rowe.

Lupan, O., S. Shishiyanu, V. Ursaki, H. Khallaf, L. Chow, T. Shishiyanu, V. Sontea, E. Monaico, and S. Railean. 2009. "Synthesis of Nanostructured Al-Doped Zinc Oxide Films on Si for Solar Cells Applications." *Solar Energy Materials and Solar Cells* 93:1417.

Ohtaki, M., K. Araki, and K. Yamamoto. 2009. "High Thermoelectric Performance of Dually Doped ZnO Ceramics." *The Journal of Electronic Materials* 38:1234.

Ohtaki, M., T. Tsubota, K. Eguchi, and H. Arai. 1996. "High-Temperature Thermoelectric Properties of (Zn1–xAlx)O." *Journal of Applied Physics* 79:1816.

Özgür, Ü., Y. I. Alivov, C. Liu, A. Teke, M. A. Reshchikov, S. Doğan, V. Avrutin, S.-J. Cho, and H. Morkoç. 2005. "A Comprehensive Review of ZnO Materials and Devices." *Journal of Applied Physics* 98:041301.

Senda, T., and R. C. Bradt. 1990. "Grain Growth in Sintered ZnO and ZnO-Bi_2O_3 Ceramics." *The Journal of the American Ceramic Society* 73:106.

Sernelius, B. E., K. F. Berggren, Z. C. Jin, I. Hamberg, and C. G. Granqvist. 1988. "Band-Gap Tailoring of ZnO By Means Of Heavy Al Doping." *Physical Review B* 37:10244.

Shirouzu, K., T. Ohkusa, M. Hotta, N. Enomoto, and J. Hojo. 2007. "Distribution and Solubility Limit of Al in Al_2O_3-Doped ZnO Sintered Body." *Journal of the Ceramic Society of Japan* 115:254.

Singh, A. V., R. M. Mehra, A. Yoshida, and A. Wakahara. 2004. "Doping Mechanism in Aluminum Doped Zinc Oxide Films." *Journal of Applied Physics* 95:3640.

Snyder, G. J., and E. S. Toberer. 2008. "Complex Thermoelectric Materials." *Nature Materials* 7:105.

Tsubota, T., M. Ohtaki, K. Eguchi, and H. Arai. 1997. "Thermoelectric Properties of Al-Doped ZnO as a Promising Oxide Material for High-Temperature Thermoelectric Conversion." *Journal of Materials Chemistry* 7:85.

Vanheusden, K., C. H. Seager, W. L. Warren, D. R. Tallant, and J. A. Voigt. 1996. "Correlation between Photoluminescence and Oxygen Vacancies in ZnO Phosphors." *Applied Physics Letters* 68:403.

Willander, M., O. Nur, J. R. Sadaf, M. I. Qadir, S. Zaman, A. Zainelabdin, N. Bano, and I. Hussain. 2010. "Luminescence from Zinc Oxide Nanostructures and Polymers and Their Hybrid Devices." *Materials* 3:2643.

Zhan, Z. B., J. Y. Zhang, Q. H. Zheng, D. M. Pan, J. Huang, F. Huang, and Z. Lin. 2011. "Strategy for Preparing Al-Doped ZnO Thin Film with High Mobility and High Stability." *Crystal Growth & Design* 11:21.

Zhao, Y., Y. Yan, A. Kumar, H. Wang, W. D. Porter, and S. Priya. 2012. "Thermal Conductivity of Self-Assembled Nano-Structured ZnO Bulk Ceramics." *Journal of Applied Physics* 112:034313.